Atmos. Chem. Phys., 22, 13389–13406, 2022
https://doi.org/10.5194/acp-22-13389-2022

Atmospheric Chemistry and Physics
Open Access
EGU

Examination of brown carbon absorption from wildfires in the western US during the WE-CAN study

Amy P. Sullivan[1], Rudra P. Pokhrel[2,a,b], Yingjie Shen[2], Shane M. Murphy[2], Darin W. Toohey[3], Teresa Campos[4], Jakob Lindaas[1], Emily V. Fischer[1], and Jeffrey L. Collett Jr.[1]

[1]Department of Atmospheric Science, Colorado State University, Fort Collins, CO 80523, USA
[2]Department of Atmospheric Science, University of Wyoming, Laramie, WY 82071, USA
[3]Department of Atmospheric and Oceanic Sciences, University of Colorado – Boulder, Boulder, CO 80309, USA
[4]Atmospheric Chemistry Division, National Center for Atmospheric Research, Boulder, CO 80307, USA
[a]now at: Cooperative Institute for Research in Environmental Sciences, University of Colorado, Boulder, CO 80309, USA
[b]NOAA Chemical Science Laboratory, Boulder, CO 80305, USA

Correspondence: Amy P. Sullivan (sullivan@atmos.colostate.edu)

Received: 28 June 2022 – Discussion started: 1 July 2022
Revised: 23 September 2022 – Accepted: 25 September 2022 – Published: 18 October 2022

Abstract. Light absorbing organic carbon, or brown carbon (BrC), can be a significant contributor to the visible light absorption budget. However, the sources of BrC and the contributions of BrC to light absorption are not well understood. Biomass burning is thought to be a major source of BrC. Therefore, as part of the WE-CAN (Western Wildfire Experiment for Cloud Chemistry, Aerosol Absorption and Nitrogen) study, BrC absorption data were collected on board the National Science Foundation/National Center for Atmospheric Research (NSF/NCAR) C-130 aircraft as it intercepted smoke from wildfires in the western US in July–August 2018. BrC absorption measurements were obtained in near real-time using two techniques. The first coupled a particle-into-liquid sampler (PILS) with a liquid waveguide capillary cell and a total organic carbon analyzer for measurements of water-soluble BrC absorption and WSOC (water-soluble organic carbon). The second employed a custom-built photoacoustic aerosol absorption spectrometer (PAS) to measure total absorption at 405 and 660 nm. The PAS BrC absorption at 405 nm (PAS total Abs 405 BrC) was calculated by assuming the absorption determined by the PAS at 660 nm was equivalent to the black carbon (BC) absorption and the BC aerosol absorption Ångström exponent was 1. Data from the PILS and PAS were combined to investigate the water-soluble vs. total BrC absorption at 405 nm in the various wildfire plumes sampled during WE-CAN. WSOC, PILS water-soluble Abs 405, and PAS total Abs 405 tracked each other in and out of the smoke plumes. BrC absorption was correlated with WSOC (R^2 value for PAS = 0.42 and PILS = 0.60) and CO (carbon monoxide) (R^2 value for PAS = 0.76 and PILS = 0.55) for all wildfires sampled. The PILS water-soluble Abs 405 was corrected for the non-water-soluble fraction of the aerosol using the calculated UHSAS (ultra-high-sensitivity aerosol spectrometer) aerosol mass. The corrected PILS water-soluble Abs 405 showed good closure with the PAS total Abs 405 BrC with a factor of $\sim$ 1.5 to 2 difference. This difference was explained by particle vs. bulk solution absorption measured by the PAS vs. PILS, respectively, and confirmed by Mie theory calculations. During WE-CAN, $\sim$ 45 % (ranging from 31 % to 65 %) of the BrC absorption was observed to be due to water-soluble species. The ratio of BrC absorption to WSOC or ΔCO showed no clear dependence on fire dynamics or the time since emission over 9 h.

1 Introduction

Organic compounds can comprise a large fraction of PM (particulate matter) mass (Kanakidou et al., 2005; Zhang et al., 2007). Organic carbon can be directly emitted or formed in the atmosphere from a variety of sources. This leads to organic aerosol particles composed of a number of compounds that range from insoluble to highly water-soluble and that can scatter or absorb light (Jacobson et al., 2000; Saxena and Hildemann, 1996, and references therein).

The portion of organic carbon that is light-absorbing has been referred to as brown carbon (BrC) due to its yellow or brown color when concentrated, and it is likely to be a significant contributor to the visible light-absorption budget (Andreae and Gelencsér, 2006). Recent modeling studies have predicted a non-negligible effect on the Earth's radiation balance from BrC (Feng et al., 2013; Zhang et al., 2017, 2020). Global measurements have shown that BrC can contribute up to 48 % of the overall warming effect by absorbing carbonaceous aerosols (Zeng et al., 2020). BrC may also suppress photolysis rates of some chemical reactions, including decreasing surface ozone concentrations in certain locations, due to its ability to absorb at ultraviolet wavelengths (Jo et al., 2016). Some portion of BrC is likely composed of toxins, such as nitro- and oxy-aromatic species, suggesting BrC could also have health impacts (Desyaterik et al., 2013; Verma et al., 2015; Zhang et al., 2013). BrC itself is thought to have both primary and secondary sources. Particles from biomass burning or incomplete combustion of fossil fuels generally contain significant amounts of BrC (e.g., Chakrabarty et al., 2010; Hoffer et al., 2006; Kirchstetter et al., 2004; Kirchstetter and Thatcher, 2012; Lack et al., 2012; Lukács et al., 2007). Laboratory studies have observed production of BrC from a number of formation processes. This has included heterogenous reactions of isoprene on acidic aerosol particles, a variety of aqueous-phase reactions, and reactions of organic compounds in acidic solutions (e.g., Hoffer et al., 2006; Limbeck et al., 2013; Sareen et al., 2010; Updyke et al., 2012). However, there is still limited information on the contribution of BrC to total light absorption and the sources of BrC as there are few ambient measurements.

Total absorption measurements (black carbon (BC) + BrC) at multiple wavelengths can be used to determine BrC absorption due to the strong wavelength dependence of BrC. This requires the assumptions that (1) the absorption Ångström exponent (AAE) for BC is known, (2) AAE is constant with wavelength, and (3) BrC does not absorb at longer wavelengths. The AAE for BC is well constrained at 1 in the visible and near-infrared wavelengths (Moosmüller et al., 2009). The BrC absorption at other wavelengths is then found by the difference from the extrapolated BC AAE (Lack and Langridge, 2013; Mohr et al., 2013). This approach can be applied to any technique that measures absorption at multiple wavelengths, including photoacoustic spectroscopy (PAS).

BrC can also be quantified by isolating the BrC chromophores by the extraction of particles in solvents, such as water or methanol, in order to separate them from the insoluble BC and then measuring the light absorption of the soluble organic chromophores (Hecobian et al., 2010). This is the only direct method to separate and quantify BrC, as the light absorption from liquid extracts does not suffer from interferences by BC, as they can be isolated by dissolution. A spectrophotometer with an UV/Vis (ultraviolet/visible) light source can provide high spectral resolution over a wide wavelength range from 200 to 800 nm. In addition, when coupled with a long-path liquid waveguide capillary absorption cell (LWCC), it also provides a highly sensitive measurement. This technique can be used offline with filters or online with an aerosol collection device such as a particle-into-liquid sampler (PILS) (e.g., Hecobian et al., 2010; Liu et al., 2013, 2014, 2015; Zhang et al., 2011, 2013).

Here we report BrC absorption data from a PAS and PILS–LWCC–TOC (total organic carbon) system to compare total vs. water-soluble BrC absorption in wildfire smoke. Data are from smoke plume penetrations during the Western Wildfire Experiment for Cloud Chemistry, Aerosol Absorption and Nitrogen (WE-CAN), an aircraft-based study focused on investigating the chemistry and transformation of emissions from wildfires in the western US. We examine the relationship between the BrC absorption and species known to be from biomass burning. We discuss how parameters such as aging and fire dynamics might influence BrC absorption from wildfires.

2 Methods

2.1 The airborne mission

The WE-CAN campaign was a multi-investigator study conducted on board the National Science Foundation/National Center for Atmospheric Research (NSF/NCAR) C-130 aircraft. The C-130 was operated out of Boise, Idaho (ID), from 20 July to 31 August 2018. A suite of instruments was deployed for measurements of aerosol and trace gas composition. A total of 16 research flights sampled wildfire smoke over the western US to characterize emissions, mixing, chemical transformations, and transport. Figure 1 presents a map of the flight transects and locations of the wildfires sampled. (We exclude flight RF14, which was conducted off the coast of California (CA) to sample a stratus deck impacted by smoke, and flight RF16, which consisted of an intercomparison performed near Boise between WE-CAN and BB-FLUX (Biomass Burning Flux Measurements of Trace Gases and Aerosols) common measurements.) More information on each wildfire including the type of fuel consumed is available in the WE-CAN field catalog (https://catalog.eol.ucar.edu/we-can, last access: 13 Decem-

ber 2021). WE-CAN sampled both fresh and aged (for flights RF05 and RF08 along with parts of flights RF07 and RF13) emissions from smoke for wildfires burning in CA, Oregon (OR), Washington (WA), ID, Montana (MT), Utah (UT), and Nevada (NV). The general sampling strategy was to circle the wildfire at the source and then follow the smoke downwind using a multiple transect search and rescue pattern to examine smoke evolution. Typically, wildfire smoke plumes were sampled in the free troposphere between 3 and 5 km during the early afternoon to evening periods (20:00 to 02:00 UTC or 14:00 to 20:00 LT). Flight RF08 and part of flight RF07 were exceptions as the aircraft sampled the boundary layer (below 2 km) over the Central Valley of CA.

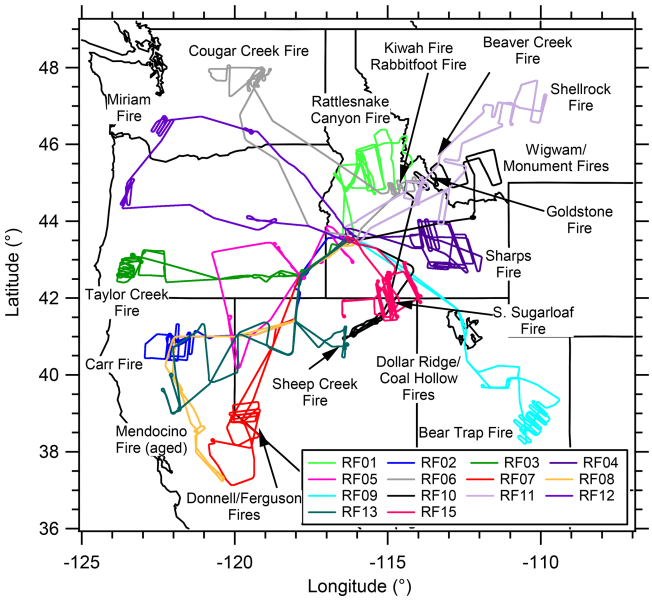

Figure 1. Map showing the flight paths and locations of the wildfires sampled during WE-CAN used in this analysis.

2.2 Particle collection

During WE-CAN, we deployed two particle-into-liquid sampler (PILS) systems. A PILS is an aerosol collection device that continuously collects ambient particles into purified water (Orsini et al., 2003). After particles are grown inside the body of the PILS by water condensation in a supersaturated water vapor environment, formed through mixing the ambient air sample with saturated air (100 % relative humidity) at higher temperature, the particles are collected by an impactor. The impactor plate is continually washed off by a flow of liquid passed over the impactor, providing a liquid sample containing dissolved aerosol particles which can be analyzed by various methods. Each PILS system sampled from their own submicron aerosol inlet (SMAI) (Craig et al., 2013a, b, 2014; Moharreri et al., 2014) mounted to the belly of the NSF/NCAR C-130. The size-cut for each PILS was provided by a nonrotating MOUDI impactor stage with a 50 % transmission efficiency of 1 µm aerodynamic diameter (i.e., PM_1) at 1 atm ambient pressure (Marple et al., 1991). The flowrate of 15 L min^{-1} was sampled by each PILS through the inlet and MOUDI stage. An activated carbon parallel plate denuder (Eatough et al., 1993) was situated upstream of both PILS systems to remove organic gases. In addition, for PILS2 two honeycomb denuders coated with sodium carbonate and phosphorous acid were used to remove inorganic acidic and basic gases in order to limit possible positive artifacts from dissolving in the PILS collection liquid. PILS1 was connected to a LWCC (liquid waveguide capillary cell) and TOC (total organic carbon) analyzer for near-real-time measurement of water-soluble BrC absorption and WSOC (water-soluble organic carbon), respectively. PILS2 was coupled to a Bretchel fraction collector system (Sorooshian et al., 2006) to provide liquid samples for additional offline analysis.

For PILS1, a valve upstream of the PILS was manually closed periodically for 10 min forcing the airflow through a Teflon filter allowing for a measurement of the background in near real-time. The liquid sample obtained from PILS1 was then pushed through a 0.2 µm PTFE liquid filter at a flowrate of 1.2 mL min^{-1} by a set of syringe pumps with 1 mL syringes to ensure any insoluble particles were removed before passing through the LWCC and TOC analyzer.

A LWCC with a 2.5 m path length (World Precision Instruments, Sarasota, FL) was employed. An absorption spectrometer (FLAME-T-UV-VIS, Ocean Optics, Largo, FL) and dual deuterium and tungsten halogen light source (DH-mini, Ocean Optics, Largo, FL) were coupled to the LWCC via fiber-optic cables. The OceanView Spectroscopy Software was used to record absorption spectra over a range from 200 to 800 nm. In this paper we present the absorption determined at 365 and 405 nm. This wavelength-dependent absorption was calculated following the method outlined in Hecobian et al. (2010). A 16 s integrated measurement of water-soluble absorption with a limit of detection (LOD) of 0.1 Mm^{-1} was obtained.

A Sievers model M9 portable TOC analyzer (Suez Waters Analytical Instruments, Boulder, CO) was used for the WSOC measurement. This analyzer converts organic carbon in the liquid sample to carbon dioxide using chemical oxidation with ammonium persulfate and ultraviolet light. The carbon dioxide formed is then measured by conductivity. The amount of OC present in the sample is proportional to the increase in conductivity observed. The analyzer was run in turbo mode providing a 4 s integrated measurement of WSOC with a LOD of 0.1 µg C m^{-3}.

For PILS2, a valve upstream of the PILS was manually closed periodically for 10 min forcing the airflow through a HEPA filter allowing for measurement of the background in near real-time. The liquid sample obtained from PILS2 was pushed into the fraction collector vials at a flowrate of 0.65 mL min^{-1} by a peristaltic pump for collection of

$\sim$ 1.2 mL of liquid sample per vial. Each fraction collector carousel holds 72 1.5 mL polypropylene vials (MicroSolv Technology Corporation, Leland, NC). Vials were fitted with pre-slit caps and used as supplied. The fraction collector program was set to allow continuous collection of 2 min integrated samples and was manually started after take-off. Carousels were pre-loaded before flight and then manually switched out as they were filled. The vials were unloaded from the carousels at the end of each flight, recapped with solid caps (MicroSolv Technology Corporation), packed in coolers with ice packs, and shipped back to Colorado State University to be stored in a 2 °C cold room until analysis began following completion of the study.

2.3 Offline analysis

Each fraction collector vial was brought to room temperature and then analyzed for anhydrosugars, as well as cations. For each analysis, 300 µL aliquots were transferred to polypropylene vials. Only levoglucosan, water-soluble potassium, and ammonium are discussed here, and their analytical methods are explained below.

The levoglucosan analysis was performed on a Dionex DX-500 series ion chromatograph with pulsed amperometric detection via an ED-50/ED-50A electrochemical cell. This cell includes two electrodes: a "standard" gold working electrode and a pH-Ag/AgCl (silver/silver chloride) reference electrode. A sodium hydroxide gradient and a Dionex CarboPac PA-1 column (4 × 250 mm) were employed for the separation. The complete run time was 59 min with an injection volume of 100 µL. More details on the method can be found in Sullivan et al. (2011a, b, 2014, 2019). Only levoglucosan could be detected in the WE-CAN samples (other less abundant anhydrosugars were too low to detect in the PILS samples) and did not require background correction. The LOD for levoglucosan based on a sample collection time of 2 min and air flowrate of 15 L min^{-1} was determined to be less than approximately 0.10 ng m^{-3}.

A Dionex ICS-3000 ion chromatograph equipped with a conductivity detector was used to measure water-soluble potassium and ammonium. An eluent generator provided a concentration of 20 mM methanesulfonic acid at a flowrate of 0.5 mL min^{-1} to perform the separation on a Dionex IonPac CS12A analytical column (3 × 150 mm). The complete run time was 17 min with an injection volume of 190 µL. A blank correction was necessary for both of these species unlike levoglucosan. Therefore, their concentrations were corrected by using the average of all background samples collected during a specific flight. For water-soluble potassium and ammonium, the LOD was 1 ng m^{-3}.

2.4 Photoacoustic aerosol absorption spectrometer

A custom-built PAS was used to measure total aerosol absorption at 405 and 660 nm (Foster et al., 2019) every 1 s during WE-CAN. The PAS measures aerosol light absorption at near-ambient conditions by heating particles using a controlled light source and detecting the resulting sound wave. It can be subject to interference by gaseous absorbers and is sensitive to variations in relative humidity, temperature, and pressure (Arnott et al., 1999; Langridge et al., 2013). The PAS sampled from a solid diffuser inlet (SDI) mounted on the front right side of the NSF/NCAR C-130. Aerosol passed through a cyclone impactor before entering the PAS to remove particles with aerodynamic diameters > 1 µm. The flowrate for the PAS was 4 L min^{-1}. Upstream of the PAS was a denuder to remove NO_x (nitrogen oxides) from the sample air, as well as a Perma Pure dryer to dry the aerosol to below 30 % relative humidity. A filter was periodically switched in-line before the PAS to remove particles and allow for a near-real-time measurement of the baseline stability. Additionally, the PAS switched between sampling with and without a thermal denuder system in-line. Only the data from sampling without the thermal denuder are presented here. The PAS BrC absorption at 405 nm (PAS total Abs 405 BrC) was calculated using Eq. (9) from Pokhrel et al. (2017). This approach assumes the absorption determined by the PAS at 660 nm was equivalent to BC absorption, the BC aerosol AAE was 1, and the absorption enhancement from lensing was constant at all wavelengths. Previous work using this approach in smoke from controlled laboratory burns found lensing could contribute a maximum of 30 % of total absorption but typically contributes much less.

2.5 Ultra-high-sensitivity aerosol spectrometer

The 1 sec particle number concentrations were measured using a rack-mounted UHSAS (ultra-high-sensitivity aerosol spectrometer). The rack-mounted UHSAS switched between sampling from the SDI inlet and a CVI (counter-flow virtual impactor) when sampling out of cloud and in cloud, respectively. We only present data for sampling out of clouds. The rack-mounted UHSAS was operated so that the flow could be manually lowered by the in-flight operator when the NSF/NCAR C-130 flew through smoke plumes to allow the UHSAS to stay within its optimum concentration measurement range. The UHSAS measures particles in the 0.06–1 µm range. The particle size bins for the UHSAS were calibrated using ammonium sulfate rather than traditional PSL (polystyrene latex) spheres. Particle mass concentrations for PM_1 were calculated by summing all size bins and then multiplying by 1.4 g cm^{-3} to account for particle density.

2.6 Other measurements

In the following analysis, we focus on characterizing the BrC absorption in smoke from wildfires in the western US sampled during WE-CAN. Other airborne measurements used in this analysis include meteorological data and coordinates provided by the Research Aviation Facility (RAF) as part of

the C-130 instrumentation package (https://data.eol.ucar.edu/project/WE-CAN, last access: 13 December 2021) and 1 Hz carbon monoxide (CO) determined by a vacuum UV resonance fluorescence method (Gerbig et al., 1999). All data presented in our analysis are reported at 1 atm and 273 K. Data from all species have been averaged to match the 2 min collection time of the PILS-fraction collector system.

2.7 Mie calculation

Mie calculations were performed by putting the complex refractive index ($m = n + ik$) into Mie code to obtain the absorption efficiency (Q) and then further calculate the absorption coefficient using Eq. (1) (Liu et al., 2013). The real part of the refractive index (n) was set to be 1.55, and the imaginary part was calculated using Eq. (2) (Liu et al., 2013).

$$\beta\left(\lambda, D_{\mathrm{p}}\right) = \frac{3}{2} \cdot \frac{Q \cdot \mathrm{WSOC}}{D_{\mathrm{p}} \cdot \rho} \tag{1}$$

$$k = \frac{\rho\lambda \cdot \mathrm{H_2O\_}\beta(\lambda)}{4\pi \cdot \mathrm{WSOC}} \tag{2}$$

In Eqs. (1) and (2), λ is the wavelength, D_{p} is the diameter of the particle, β is the absorption coefficient (referred to as the Mie-calculated water-soluble absorption hereinafter), Q is the absorption efficiency, WSOC is the water-soluble organic carbon mass concentration measured by the PILS, and $\mathrm{H_2O\_}\beta(\lambda)$ is the water-soluble light absorption coefficient measured by the PILS. The particle density (ρ) was assumed to be 1.4 g cm^{-3}. The plume averaged particle size distribution (measured by the UHSAS) was used in the calculation. The Mie-calculated water-soluble absorption was determined for each size bin in order to obtain the most accurate results. Mie-calculated total absorption was further calculated by multiplying the Mie-calculated water-soluble absorption by (UHSAS mass)/(WSOC · 1.6), where the factor of 1.6 was to convert WSOC to WSOM (water-soluble organic matter) (Duarte et al., 2019; Yttri et al., 2007).

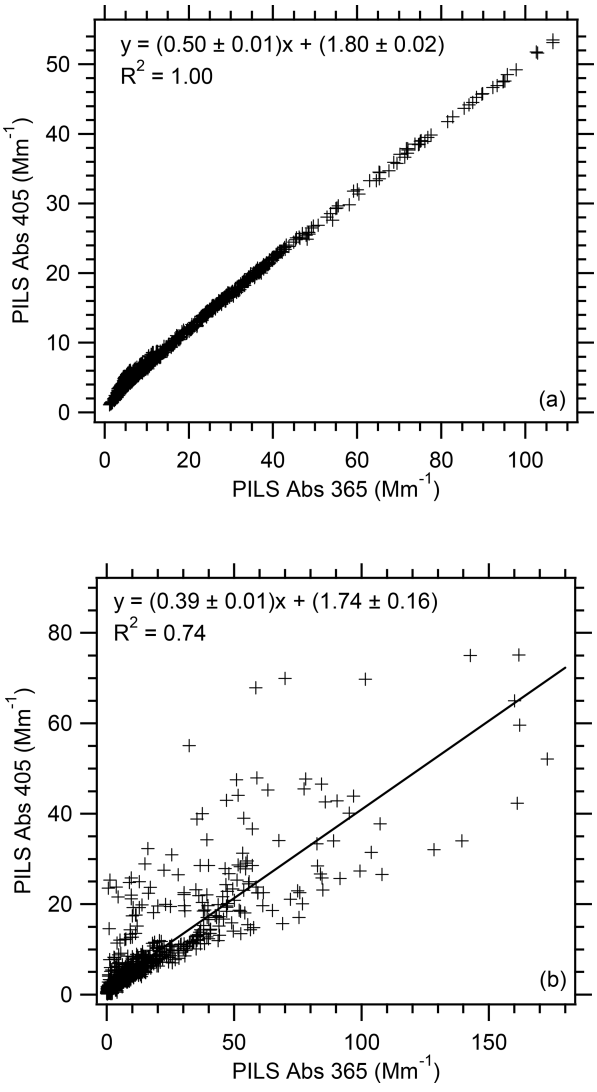

Figure 2. Correlation of PILS water-soluble Abs 405 vs. PILS water-soluble Abs 365 for WE-CAN **(a)** flight RF02 and **(b)** flight RF11. Uncertainties with the least square regressions are 1 standard deviation.

3 Results and discussion

3.1 Overview

Most previous studies employing a LWCC to determine water-soluble absorption examine the absorption at 365 nm (e.g., Hecobian et al., 2010; Zhang et al., 2011, 2013). But here in order to explore the relationship between the water-soluble and total absorption determined by the PILS and PAS, respectively, we focus on the absorption at 405 nm determined by the LWCC. Using as examples flight RF02, which sampled the Carr Fire smoke plume, and flight RF11, which sampled the Goldstone, Rabbit Foot, Beaver Creek, and Shellrock Fire smoke plumes, Fig. 2a and b show the relationship of the PILS water-soluble Abs 405 vs. Abs 365. Absorption values at these two wavelengths are correlated (R^2 values from 0.70 to 1.00 based on all individual WE-CAN flights), but the absorption measured at 405 nm was about half of that observed at 365 nm (slope average 0.45 and range from 0.39 to 0.52 across all individual WE-CAN flights). We selected these two flights to cover the range in the relationships observed during WE-CAN. The lower correlation for flight RF11 is likely due to the narrower plumes being sampled compared to the broader plumes observed in flight RF02. This difference related to narrow vs. broad plumes was observed throughout the various wildfires sampled during WE-CAN.

Figure 3 shows example time series for WSOC, PILS water-soluble Abs 405, and PAS total Abs 405 BrC from

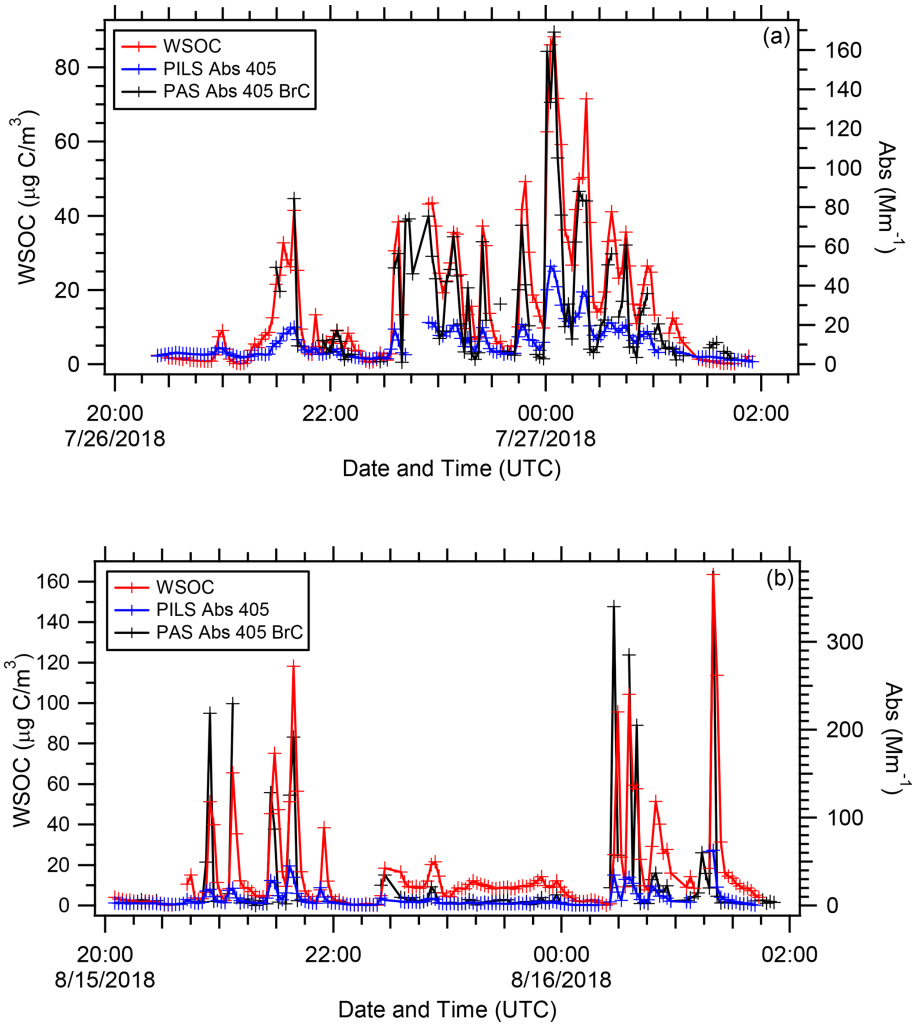

Figure 3. Time series of WSOC, PILS water-soluble Abs 405, and PAS total Abs 405 BrC for WE-CAN **(a)** flight RF02 and **(b)** flight RF11.

the same two flights as above. It was observed that all three parameters tracked each other in and out of the smoke plumes. During WE-CAN, the average value ± standard deviation for WSOC, PILS water-soluble Abs 405, and PAS total Abs 405 BrC were $13.35 \pm 16.80\,\mu g\,C\,m^{-3}$, 6.06 ± 6.88, and $22.02 \pm 49.16\,Mm^{-1}$, respectively. The water-soluble absorption determined by the PILS was lower than the total absorption determined by the PAS. This pattern was consistently observed for all the wildfires sampled throughout WE-CAN.

3.2 Relationship between total and water-soluble BrC absorption

To further explore the relationship between total and water-soluble BrC absorption, we examine the relationship between PAS total Abs 405 BrC and UHSAS mass for flights RF02 and RF11. There is a strong correlation between PAS total Abs 405 BrC and UHSAS mass (Fig. 4). Therefore, the PILS water-soluble Abs 405 can be corrected for the non-water-soluble fraction of the aerosol using the UHSAS mass. This was achieved by multiplying the PILS water-soluble Abs 405 by $1/((WSOC \cdot 1.6)/(UHSAS\ mass))$ or $(UHSAS\ mass)/(WSOC \cdot 1.6)$. This approach assumes the characteristics of the non-water-soluble components of OC are identical to those of the water-soluble components of OC.

Correcting the PILS water-soluble Abs 405 by the UHSAS mass showed good closure with the PAS total Abs 405 BrC but with a factor of ~ 1.5 to 2 difference between the PILS water-soluble Abs 405 corrected and PAS total Abs 405 BrC (Fig. 4c and d). This is also similar to results obtained from the sampling of wildfire smoke during the FIREX (Fire Influence on Regional and Global Environments Experiment) campaign, where there was a ratio of 3.2 between PAS Abs 405 BrC and water-soluble Abs 405 determined from offline LWCC analysis of filter samples (Zeng et al., 2020). This factor difference in both the WE-CAN and FIREX data is likely due to the differences in particle vs. bulk solution ab-

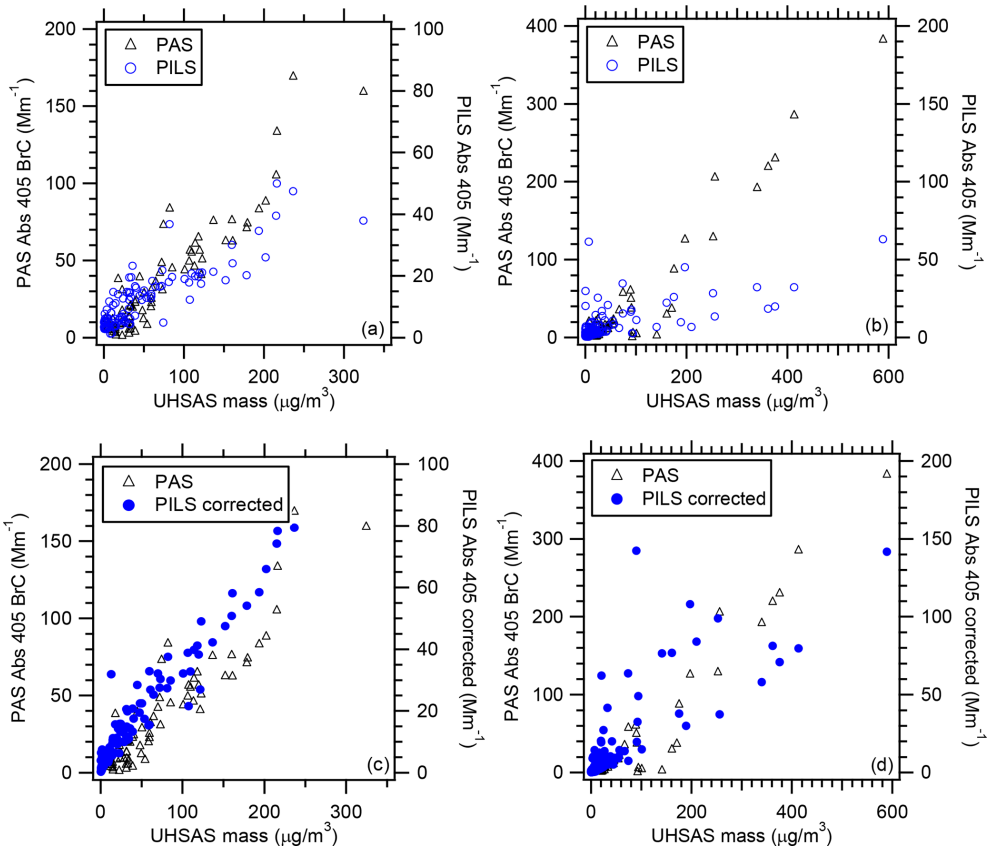

Figure 4. Correlation of PAS total Abs 405 BrC and PILS water-soluble Abs 405 vs. UHSAS mass for WE-CAN **(a)** flight RF02 and **(b)** flight RF11. Correlation of PAS total Abs 405 BrC and PILS water-soluble Abs 405 corrected for the non-water-soluble fraction of the aerosol using the UHSAS mass for WE-CAN **(c)** flight RF02 and **(d)** flight RF11. In plot **(a)**, the equations for the fit and R^2 value for PAS are $y = (0.50 \pm 0.02)x - (0.03 \pm 2.29)$ and $R^2 = 0.87$ and for PILS are $y = (0.14 \pm 0.01)x + (5.58 \pm 0.65)$ and $R^2 = 0.75$, respectively. In plot **(b)**, the equations for the fit and R^2 value for PAS are $y = (0.62 \pm 0.03)x - (6.09 \pm 3.62)$ and $R^2 = 0.76$ and for PILS are $y = (0.08 \pm 0.01)x + (3.58 \pm 0.66)$ and $R^2 = 0.43$, respectively. In plot **(c)**, the equation for the fit and R^2 value for PILS are $y = (0.32 \pm 0.01)x + (3.60 \pm 0.68)$ and $R^2 = 0.94$, respectively. In plot **(d)**, the equation for the fit and R^2 value for PILS are $y = (0.24 \pm 0.01)x + (2.93 \pm 1.35)$ and $R^2 = 0.65$, respectively. Uncertainties with the least square regressions are 1 standard deviation.

sorption measured by the PAS vs. LWCC (using PILS or filter samples), respectively, and can be explained by Mie theory.

We used Mie theory to calculate the water-soluble and total particle Abs 405 (see Sect. 2.7 for details on the equations and parameters used) through each plume transect for RF02 and RF11. As shown in Fig. 5a and b, we found a slope of 1.7 to 1.8 for Mie-calculated water-soluble Abs 405 to PILS Abs 405 and 3 to 4 for Mie-calculated total Abs 405 to PILS Abs 405. This is similar to results presented in Liu et al. (2013) and based on offline LWCC analysis of filter samples collected at three sites in Georgia. In that work, a ratio of 2 for Mie-calculated water-soluble Abs 365 to measured water-soluble Abs 365 and a ratio of 3.6 for Mie-calculated total Abs 365 to measured water-soluble Abs 365 were observed. In Zeng et al. (2022), Mie theory was used to calculate the factor to convert solution to particle light absorption (i.e., ratio of Mie-calculated to measured water-soluble absorption) as a function of wavelength for the FIREX data. At 405 nm a factor of ~ 1.7 was determined, similar to what was determined from the WE-CAN data.

As a further check on the calculations performed here, the PAS Abs 405 BrC was compared to the Mie-calculated total Abs 405. Slopes ranged from 1.04 to 1.08 (Fig. 5c and d). This suggested our approach for correcting the PILS water-soluble Abs 405 for the non-water-soluble fraction, as well as to calculate the BrC absorption from the PAS Abs 405 data, was valid.

Overall, during WE-CAN $\sim 45\,\%$ (ranging from 31 % to 65 %) of the BrC absorption at Abs 405 was due to water-soluble species. This is similar to what was observed from offline LWCC analysis of water and methanol extracts from filter samples collected during sampling of biomass burning plumes as part of the DC3 (Deep Convective Clouds and Chemistry), SEAC4RS (Studies of Emissions, Atmospheric Composition, Clouds and Climate Coupling by Re-

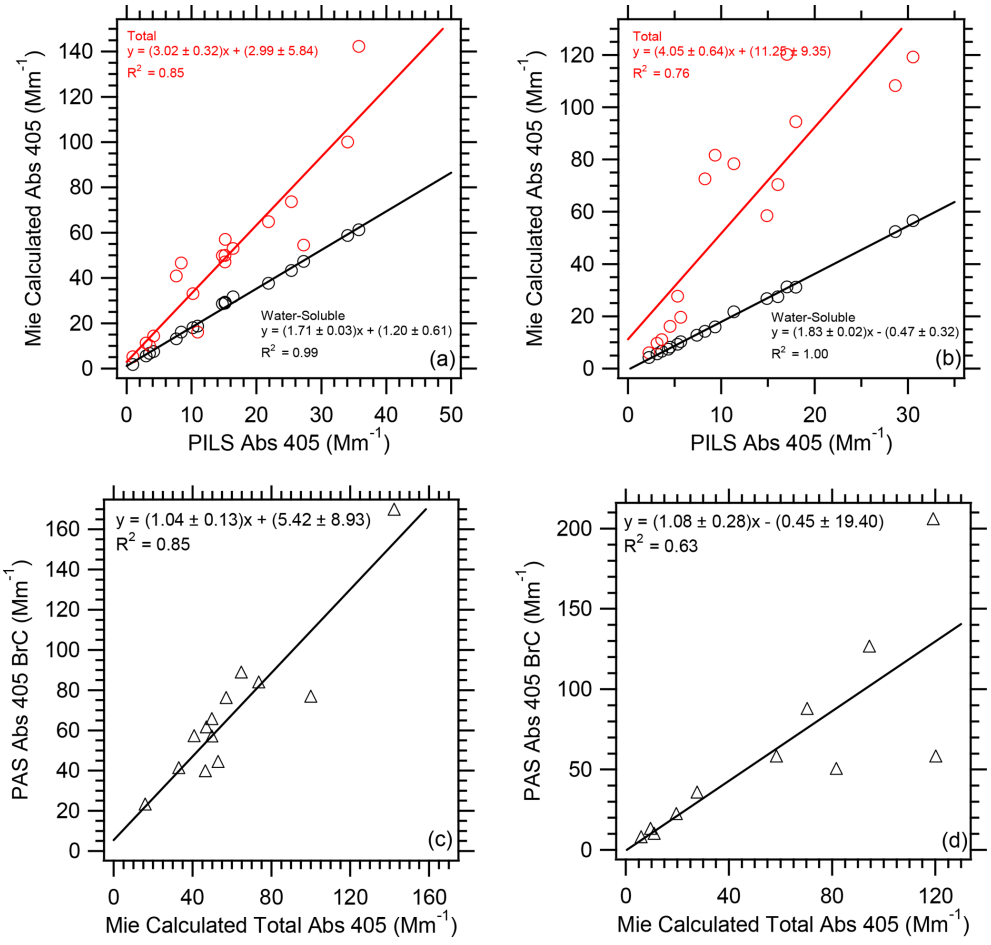

Figure 5. Correlation of Mie-calculated water-soluble and total Abs 405 vs. PILS water-soluble Abs 405 for WE-CAN **(a)** flight RF02 and **(b)** flight RF11. Correlation of PAS total Abs 405 BrC and Mie-calculated total Abs 405 for WE-CAN **(c)** flight RF02 and **(d)** flight RF11. Uncertainties with the least square regressions are 1 standard deviation.

gional Surveys), and FIREX aircraft campaigns (Forrister et al., 2015; Liu et al., 2015; Zeng et al., 2022).

3.3 BrC absorption, CO, WSOC, and levoglucosan

Using data from all WE-CAN flights, Fig. 6 shows that the PAS total Abs 405 BrC and PILS water-soluble Abs 405 are correlated with CO (R^2 value for PAS = 0.76 and PILS = 0.55). This further illustrates the importance of biomass burning as a source of BrC absorption (e.g., Andreae and Gelencsér, 2006; Chakrabarty et al., 2010; Duarte et al., 2005; Hecobian et al., 2010; Hoffer et al., 2006; Lack et al., 2012; Lukács et al., 2007), especially since more than 75 % of the WE-CAN data occurred in smoke.

Figure 7 shows that there is a correlation between BrC absorption and WSOC (R^2 value for PAS = 0.42 and PILS = 0.60). This is not surprising given that the two main sources of WSOC are typically biomass burning and secondary organic aerosol (SOA; Sullivan et al., 2006). A number of previous studies where the source of WSOC and Abs 365 was one or both of these have observed a similar correlation (e.g., Hecobian et al., 2010; Liu et al., 2015; Zhang et al., 2013).

BrC absorption has a similar relationship with CO and WSOC as the biomass burning marker levoglucosan (Simoneit et al., 1999), but there are additional features (Fig. 8). There is some variability in the ratio of levoglucosan to the PAS total Abs 405 BrC and PILS water-soluble Abs 405 between wildfires, and this leads to two branches (Branch 1 and Branch 2). This was also observed for levoglucosan vs. WSOC (not shown). While there is no overall correlation of levoglucosan vs. BrC absorption across all flights, there are correlations between these two species on an individual flight basis (e.g., R^2 value for flight RF02 = 0.76 and flight RF11 = 0.60, not shown). When data from all flights are colored by the water-soluble potassium concentration, we observe that Branch 1, which had the highest levoglucosan concentrations, also has the highest water-soluble potassium concentrations ($> 0.5\,\mu g\,m^{-3}$). Levoglucosan and BrC absorption are much more highly correlated in Branch 1 than in Branch 2 for both the PILS (R^2 values Branch 1 = 0.76

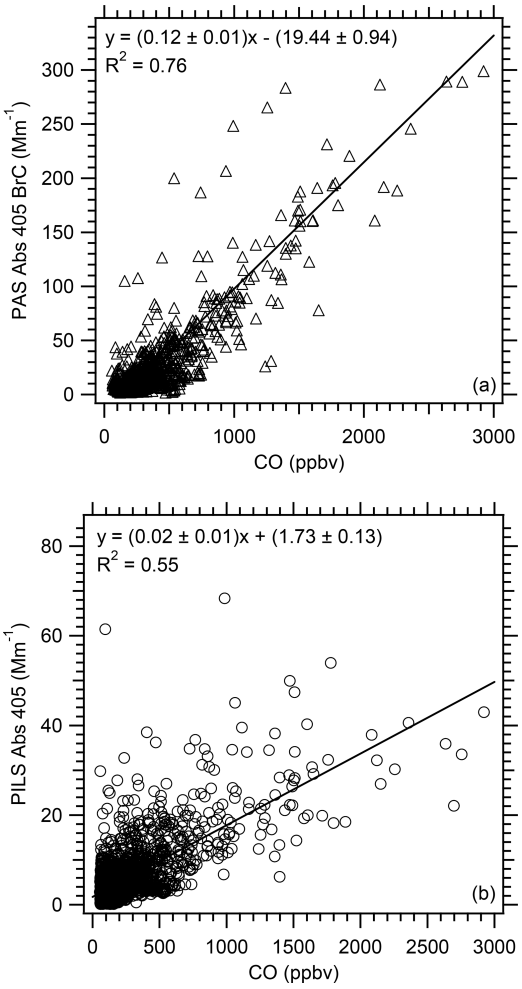

Figure 6. Correlation of **(a)** PAS total Abs 405 BrC and **(b)** PILS water-soluble Abs 405 vs. CO for all WE-CAN flights used in this analysis. Uncertainties with the least square regressions are 1 standard deviation.

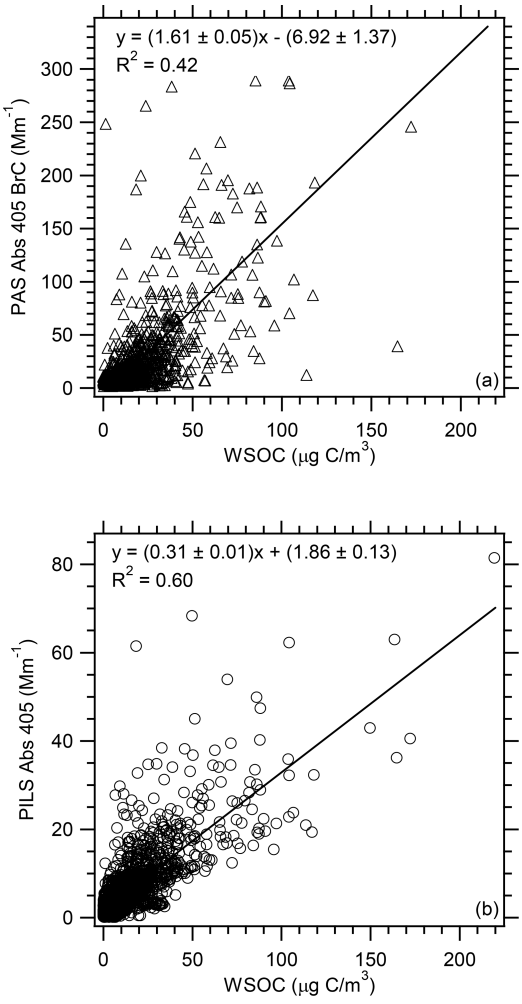

Figure 7. Correlation of **(a)** PAS total Abs 405 BrC and **(b)** PILS water-soluble Abs 405 vs. WSOC for all WE-CAN flights used in this analysis. Uncertainties with the least square regressions are 1 standard deviation.

and Branch 2 = 0.35) and PAS (R^2 values Branch 1 = 0.60 and Branch 2 = 0.22) BrC absorption. To further examine this, the times series of PILS water-soluble Abs 405, levoglucosan, potassium, and ammonium for flights RF02 and RF11 are shown in Fig. 9. Smoke-impacted samples in flight RF02 had higher concentrations of levoglucosan and water-soluble potassium and contributed to Branch 1. The data from flight RF11 contributed to Branch 2. In addition, elevated water-soluble potassium was observed in many of the plume intercepts during flight RF02. But more elevated ammonium was observed for flight RF11, which became even more prominent in smoke intercepts after 00:00 UTC, while water-soluble potassium was relatively less abundant. While ammonium was clearly more prominent, there was no correlation observed between ammonium and PAS total Abs 405 BrC or PILS water-soluble Abs 405 for the data contributing to Branch 2 (not shown). Water-soluble potassium is a known inorganic marker for biomass burning, although it is not as specific of a marker as levoglucosan, as there are additional possible sources for water-soluble potassium (Schauer et al., 2001), and water-soluble potassium is predominately emitted during only the flaming phase of a fire (Lee et al., 2010). It is possible this difference in the timing of emissions is what leads to the different relationship of Abs 405 with levoglucosan than was observed for CO and WSOC. It has been observed in previous work looking at the size-resolved aerosol composition and single-particle measurements from wildfire plumes that water-soluble potassium and levoglucosan appear in differently sized particles than BrC and that there is non-uniform mixing of them (Di Lorenzo et al., 2018; Lee et al., 2016), which could also be a factor. These results from WE-CAN are further suggesting there may be a relationship between levoglucosan and water-soluble potassium in wildfire emissions that has not been ob-

served in other types of burning, such as prescribed burning, residential burning, or controlled laboratory burns (Sullivan et al., 2014, 2019).

3.4 Evolution of BrC absorption with plume age and fire dynamics

The time since emission (i.e., the smoke age) was estimated for all possible wildfire plumes as the distance the plume was sampled from the source divided by the average wind speed at that particular sampling altitude. Only PILS-fraction collector samples that directly overlapped with a CO plume penetration are considered. To account for dilution, we normalized the BrC absorption to three different species. We examine the ratio of BrC absorption to WSOC, ΔCO (assuming a CO background of 100 ppbv), and levoglucosan.

Figure 10a presents the ratio of PAS total Abs 405 BrC to WSOC and PILS water-soluble Abs 405 to WSOC, Fig. 10b presents the ratio of PAS total Abs 405 BrC to ΔCO and PILS water-soluble Abs 405 to ΔCO, and Fig. 10c presents the ratio of PAS total Abs 405 BrC to levoglucosan and PILS water-soluble Abs 405 to levoglucosan as a function of time since emission. To better discern any trends, Figs. S1–S3 in the Supplement show these three ratios for each smoke plume on an individual flight basis. If WSOC was lost with age due to the evaporation of more volatile components or SOA formation were occurring with time since emission, CO would be expected to be more stable. It appears, however, that a similar pattern, perhaps with a bit more scatter for Abs 405 to WSOC, is observed for all of these ratios. Within a particular wildfire, there is no clear evidence that the PILS water-soluble BrC absorption is affected by smoke age up to 9 h. For the PAS total BrC absorption, especially for the ratio to ΔCO, there appears to be a possible decrease in the ratio in the first 2 h (see Figs. S1i and S2i for flight RF15 which best covered this period), suggesting a need to further explore changes in total BrC absorption near the source region.

A number of laboratory studies suggest the initial stages of photochemical aging increase light absorption (i.e., photoenhancement). This is then followed by a decrease in light absorption (i.e., photobleaching) (Hems and Abbatt, 2018; Saleh et al., 2013; Sumlin et al., 2017; Zhao et al., 2015; Zhong and Jang, 2014). However, it is challenging to directly compare these laboratory data to the ambient data collected during WE-CAN. But analysis of laboratory and ambient biomass burning samples found low-molecular-weight (< 400 Da) BrC undergoes rapid photobleaching on timescales of a few hours, but high-molecular-weight (> 400 Da) BrC was stable for up to a few days (Di Lorenzo et al., 2017; Wong et al., 2019). This suggests that the BrC sampled during WE-CAN could be composed mainly of high-molecular-weight species.

In addition, to investigate these ratios as a function of time since emission, the WE-CAN data had to be integrated across a smoke plume in order to incorporate the PILS-fraction col-

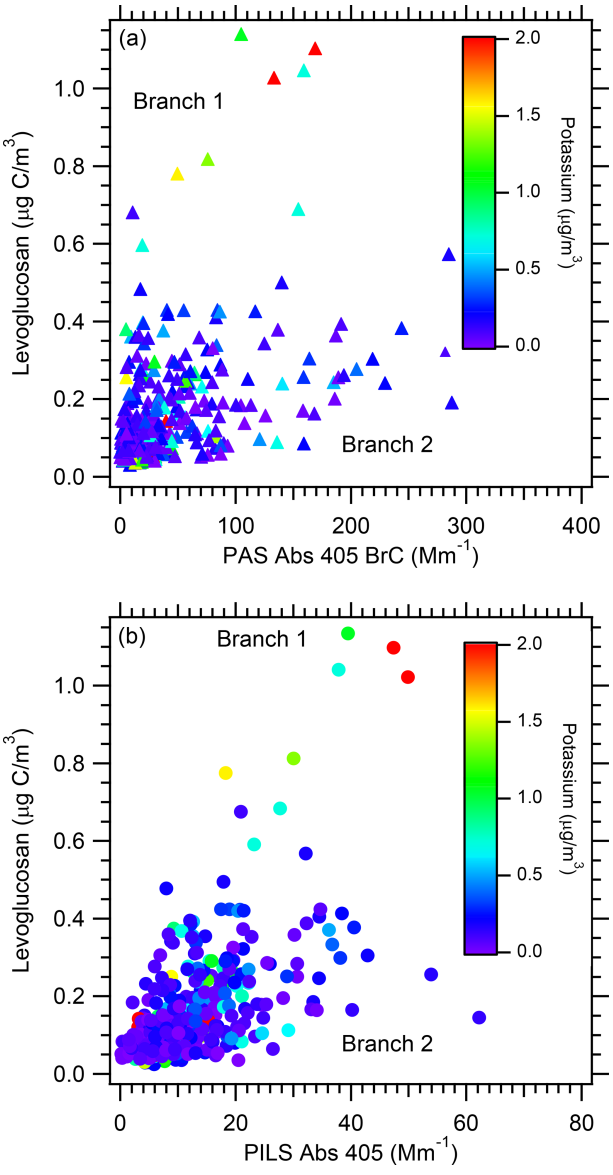

Figure 8. Correlations of levoglucosan on a carbon mass basis vs. **(a)** PAS total Abs 405 BrC and **(b)** PILS water-soluble Abs 405 for all WE-CAN flights used in this analysis with the data colored by the PILS water-soluble potassium concentrations. Branch 1 represents data with water-soluble potassium concentrations $> 0.5\,\mu g\,m^{-3}$ and Branch 2 $< 0.5\,\mu g\,m^{-3}$. In plot **(a)**, the equation for the fit and R^2 value for Branch 1 are $y = (0.006 \pm 0.001)x + (0.027 \pm 0.049)$ and $R^2 = 0.60$ and for Branch 2 $y = (0.001 \pm 0.001)x + 0.118 \pm 0.006)$ and $R^2 = 0.22$, respectively. In plot **(b)**, the equation for the fit and R^2 value for Branch 1 are $y = (0.024 \pm 0.002)x - (0.081 \pm 0.038)$ and $R^2 = 0.76$ and for Branch 2 $y = (0.006 \pm 0.001)x + (0.073 \pm 0.007)$ and $R^2 = 0.35$, respectively. Uncertainties with the least square regressions are 1 standard deviation.

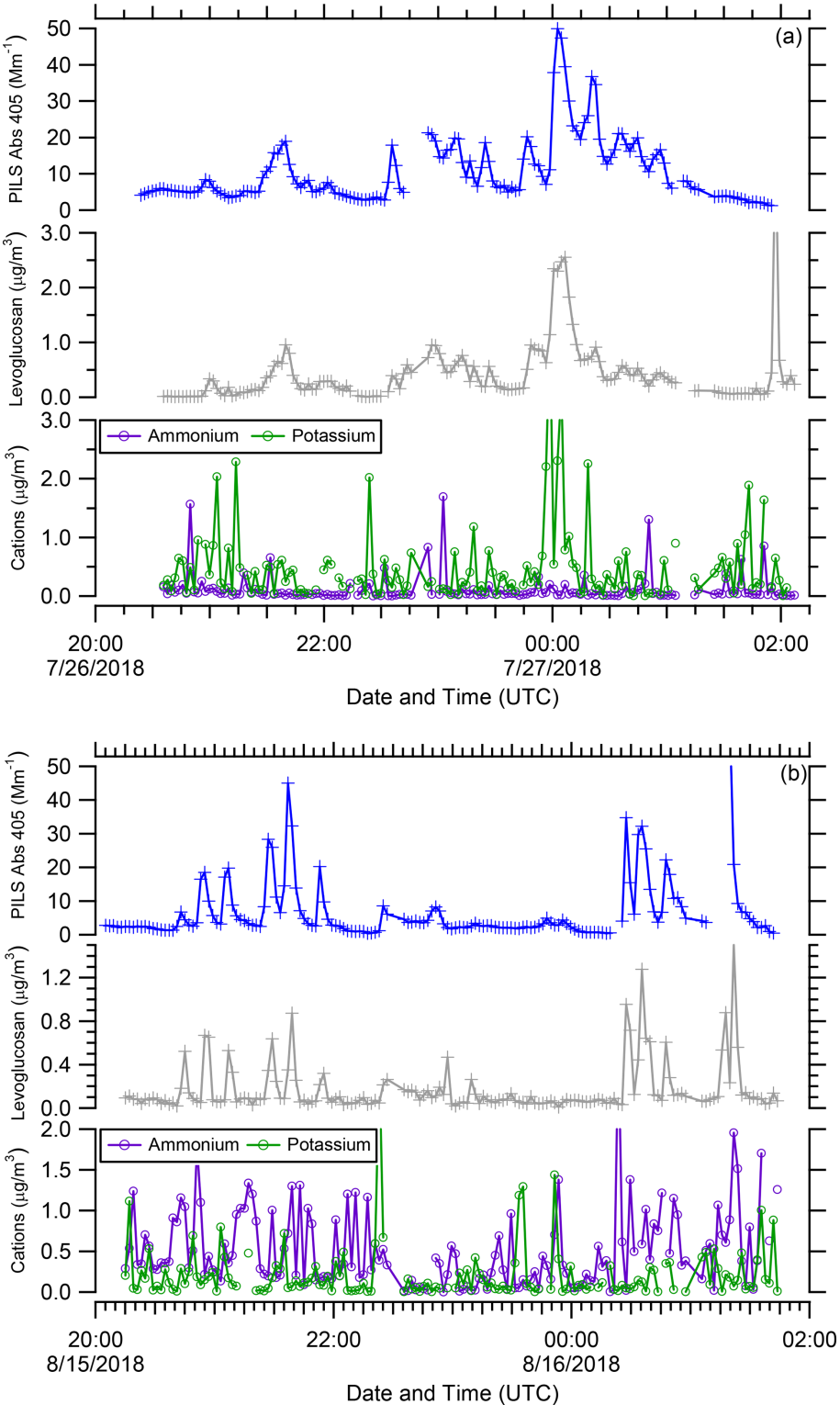

Figure 9. Time series from top to bottom of PILS water-soluble Abs 405, PILS levoglucosan, and PILS ammonium and water-soluble potassium for WE-CAN **(a)** flight RF02 and **(b)** flight RF11.

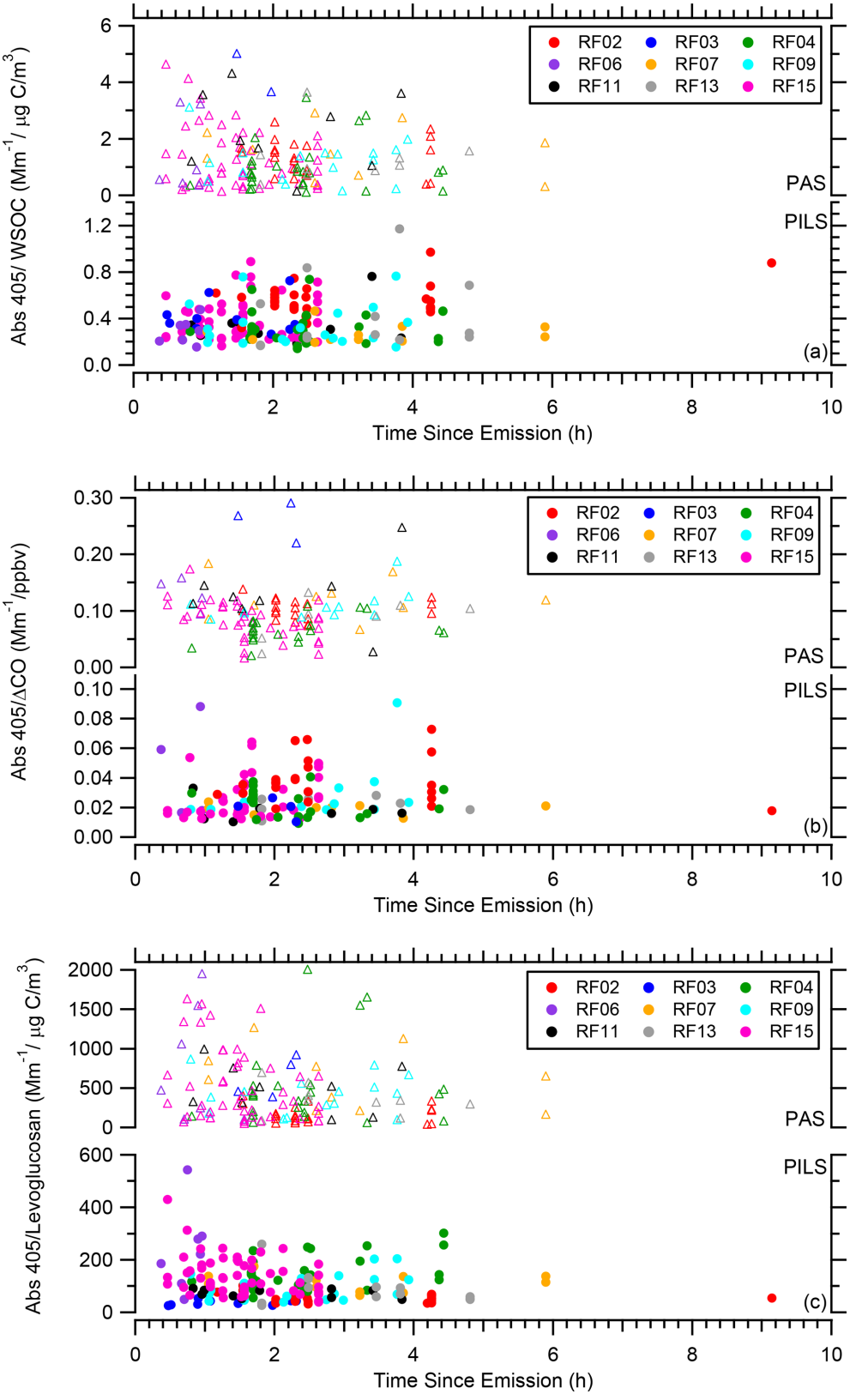

Figure 10. **(a)** Abs 405 / WSOC, **(b)** Abs 405 / ΔCO, and **(c)** Abs 405 / levoglucosan as a function of time since emission for all WE-CAN flights with the data segregated by flight. In each plot the PAS total Abs 405 BrC is on top and the PILS water-soluble Abs 405 on the bottom.

lector measurements. Of course, a smoke plume itself was dynamic with concentrations being highest in the middle of the plume and more dilute on the edges. It is possible the averaging could contribute to the observed pattern of BrC absorption not changing with age. Forrister et al. (2015), who used plume transect averages of SEAC4RS data, reported a decrease in the total Abs 365/ΔCO from ∼ 0.13 to 0.07 Mm^{-1} $ppbv^{-1}$ in 5 h for smoke from the Rim Fire. Observations of smoke during FIREX, by contrast, indicated no clear trend with plume age (Washenfelder et al., 2022; Zeng et al., 2022) in a dataset where the majority of plume ages were less than 10 h. These varying results also suggest that other factors that contribute to changes in BrC absorption over time may still need to be explored.

As these three studies all examined Abs 365, the same series of plots shown in Fig. 10 are repeated for PILS water-soluble Abs 365 and shown in Fig. S4. A similar pattern was observed at both wavelengths for the WE-CAN data. This suggests our results were not wavelength-specific and further corroborate the results observed during FIREX.

An analysis of WE-CAN data by Palm et al. (2020) looking at the evolution of organic aerosol and BrC suggested that although changes in organic aerosol were likely occurring, there was a balance between dilution-driven evaporation and subsequent formation resulting in little change over time. It is hard to compare these results to our analysis as the Palm et al. (2020) work chose to focus only on the total organic aerosol and total Abs 405 BrC and did not examine the WSOC or water-soluble Abs 405. When examining the ratio of WSOC to ΔCO as a function of time since emission (Fig. S5) during WE-CAN, there was not clear evidence for formation or loss of WSOC being observed within a particular wildfire. But a recent analysis by Zeng et al. (2022) has shown in wildfire plumes that dilution-drive evaporation was likely playing a minor role compared to the effects of ozone on BrC.

In order to investigate the possible influence of fire dynamics on BrC absorption, the modified combustion efficiency (MCE) was calculated as the change in carbon dioxide divided by the sum of the change in carbon monoxide and carbon dioxide ($\Delta CO_2/(\Delta CO+\Delta CO_2)$) on a molar basis (Ward and Radke, 1993). A higher MCE value indicates a more intense or extended flaming phase as opposed to a smoldering phase. Within a particular wildfire there appeared to be no clear dependence of the ratio of BrC absorption to WSOC, ΔCO, or levoglucosan on MCE (Figs. 11 and S6–S8), except that an overall lower Abs 405 / levoglucosan ratio was observed for the wildfires with higher MCE values (i.e., flight RF02). This further supports the relationship between the highest potassium concentrations and the levoglucosan vs. Abs 405 correlation (Fig. 8) previously discussed, as potassium is predominately emitted from the flaming phase of a fire (Echalar et al., 1995; Lee et al., 2010; Ward et al., 1991).

4 Summary

A PILS–LWCC–TOC and PAS were deployed on the NSF/NCAR C-130 research aircraft during WE-CAN to examine aerosol absorption in wildfire smoke in the western US. This was the first deployment of the PILS–LWCC–TOC on a research aircraft. The PILS allowed for a 16 s integrated measurement of the water-soluble BrC absorption and 4 s integrated measurement of WSOC. The data from the PILS and PAS were combined to investigate the water-soluble vs. total BrC absorption at 405 nm in the 20 wildfires sampled during WE-CAN. We show the following.

1. WSOC, PILS water-soluble Abs 405, and PAS total Abs 405 BrC tracked each other in and out of the smoke plumes. BrC absorption was correlated with CO (R^2 value for PAS = 0.76 and PILS = 0.55) and WSOC (R^2 value for PAS = 0.42 and PILS = 0.60) during the entire study, illustrating the importance of biomass burning as a source of BrC absorption. A similar pattern was observed for levoglucosan but with two data branches. Levoglucosan and BrC absorption were correlated (R^2 values for PAS = 0.60 and PILS = 0.76) in the first data branch, and this subset of data was also characterized by the highest observed water-soluble potassium concentrations ($> 0.5\,\mu g\,m^{-3}$). This suggests there may be a relationship between levoglucosan and water-soluble potassium in wildfire emissions that has not generally been observed in other types of burning.

2. Using the calculated UHSAS mass, the PILS water-soluble Abs 405 can be corrected to also account for the non-water-soluble fraction of the aerosol. The corrected PILS water-soluble Abs 405 showed good closure with the PAS total Abs 405 BrC but with a factor of ∼ 1.5 to 2 difference. This difference can be explained by particle vs. bulk solution absorption measured by the PAS vs. PILS, respectively, as shown by Mie theory calculations. During WE-CAN, ∼ 45 % of the BrC absorption at 405 nm was due to water-soluble species.

3. The ratio of water-soluble Abs 405 to WSOC, ΔCO, or levoglucosan showed no clear dependence on fire dynamics or the time since emission up to 9 h. The total Abs 405 BrC did show a slight decrease in the first 2 h, suggesting a need to further explore near-source evolution.

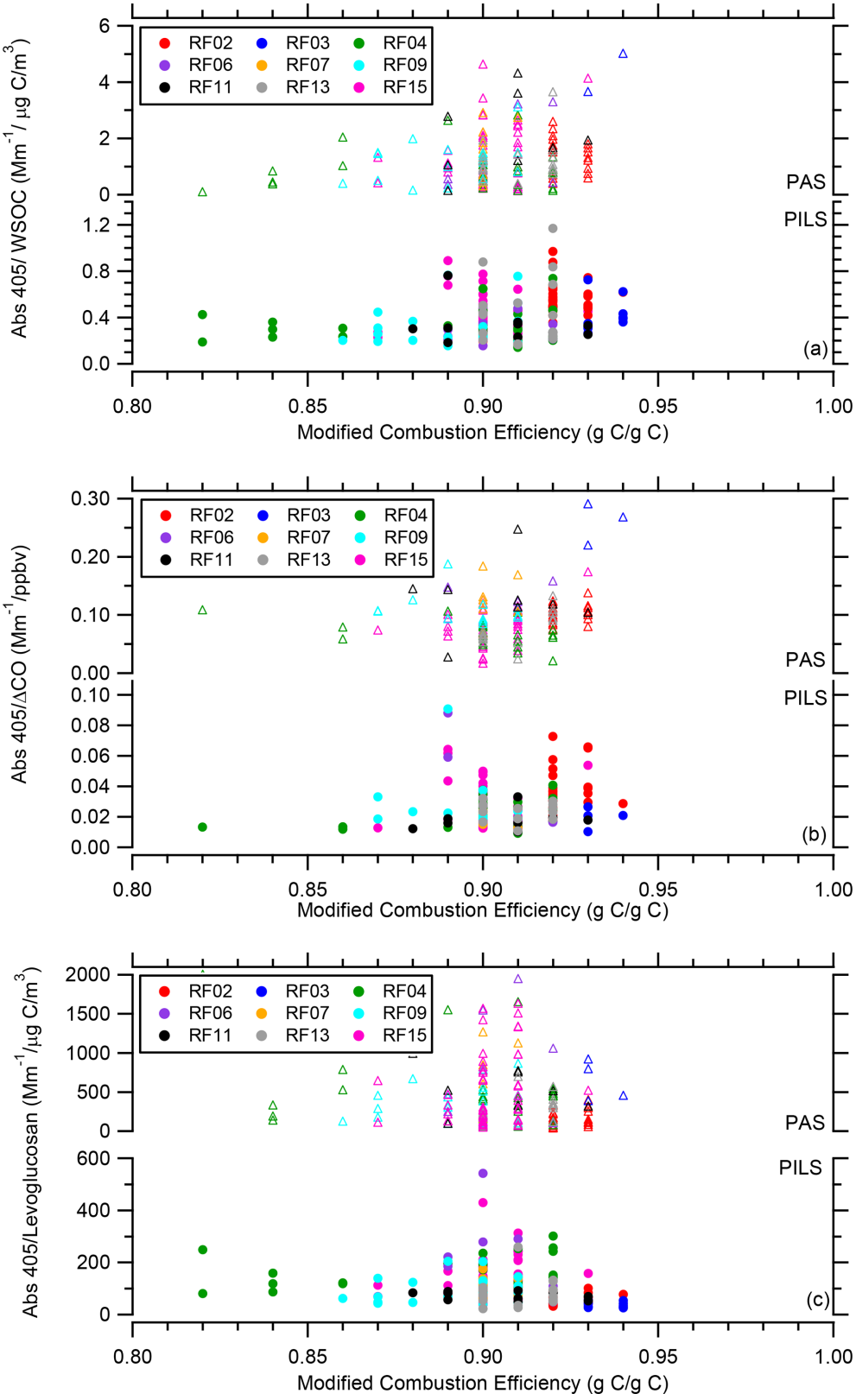

Figure 11. **(a)** Abs 405 / WSOC, **(b)** Abs 405 / ΔCO, and **(c)** Abs 405 / levoglucosan as a function of modified combustion efficiency for all WE-CAN flights with the data segregated by flight. In each plot the PAS total Abs 405 BrC is on top and the PILS water-soluble Abs 405 on the bottom.

Data availability. The WE-CAN data are provided by NCAR/EOL under sponsorship of the National Science Foundation and are available at http://data.eol.ucar.edu/master_lists/generated/we-can/ (last access: 13 December 2021). The DOI for each dataset used in this work are as follows:

PILS1: https://doi.org/10.26023/9H07-MD9K-430D (Sullivan, 2019) and https://doi.org/10.26023/CRHY-NDT9-C30V (Sullivan, 2021a);

PILS2: https://doi.org/10.26023/7TAN-TZMD-680Y (Sullivan, 2021b);

PAS: https://doi.org/10.26023/K8P0-X4T3-TN06 (Murphy, 2019);

UHSAS: https://doi.org/10.26023/BZ4F-EAC4-290W (Toohey, 2019);

CO: https://doi.org/10.26023/NNYM-Z18J-PX0Q (Campos, 2019);

Meteorological Data and Coordinates: https://doi.org/10.26023/G766-BS71-9V03 (UCAR/NCAR – Earth Observing Laboratory, 2019).

Supplement. The supplement related to this article is available online at: https://doi.org/10.5194/acp-22-13389-2022-supplement.

Author contributions. APS, SMM, DWT, EVF, and JLC Jr. designed the project. APS wrote the paper. APS, RPP, YS, SMM, DWT, TC, JL, and EVF collected and analyzed data. All authors reviewed and provided comments for the paper.

Competing interests. The contact author has declared that none of the authors has any competing interests.

Disclaimer. Publisher's note: Copernicus Publications remains neutral with regard to jurisdictional claims in published maps and institutional affiliations.

Acknowledgements. We wish to thank RAF personnel for their many contributions supporting the field deployment. We also thank Rodney J. Weber for generously providing some of the parts used in the PILS racks.

Financial support. This research has been supported by the National Science Foundation (grant no. AGS-1650786).

Review statement. This paper was edited by Sergey A. Nizkorodov and reviewed by three anonymous referees.

References

Andreae, M. O. and Gelencsér, A.: Black carbon or brown carbon? The nature of light-absorbing carbonaceous aerosols, Atmos. Chem. Phys., 6, 3131–3148, https://doi.org/10.5194/acp-6-3131-2006, 2006.

Arnott, W. P., Moosmüller, H., Rogers, C. F., Jin, T., and Bruch, R.: Photoacoustic spectrometer for measuring light absorption by aerosol: instrument description, Atmos. Environ., 33, 2845–2852, 1999.

Campos, T.: Picarro G2401-m WS-CRDS CO2, CH4, CO and H2O in situ mixing ratio observations – ICARTT format, Version 1.2, UCAR/NCAR – Earth Observing Laboratory [data set], https://doi.org/10.26023/NNYM-Z18J-PX0Q, 2019 (data available at: http://data.eol.ucar.edu/master_lists/generated/we-can/, last access: 6 May 2019).

Chakrabarty, R. K., Moosmüller, H., Chen, L.-W. A., Lewis, K., Arnott, W. P., Mazzoleni, C., Dubey, M. K., Wold, C. E., Hao, W. M., and Kreidenweis, S. M.: Brown carbon in tar balls from smoldering biomass combustion, Atmos. Chem. Phys., 10, 6363–6370, https://doi.org/10.5194/acp-10-6363-2010, 2010.

Craig, L., Moharreri, A., Schanot, A., Rogers, D. C., Anderson, B., and Dhaniyala, S.: Characterizations of Cloud Droplet Shatter Artifacts in Two Airborne Aerosol Inlets, Aerosol Sci. Tech., 47, 662–671, https://doi.org/10.1080/02786826.2013.780648, 2013a.

Craig, L., Schanot, A., Moharreri, A., Rogers, D. C., and Dhaniyala, S.: Design and Sampling Characteristics of a New Airborne Aerosol Inlet for Aerosol Measurements in Clouds, J. Atmos. Ocean. Tech., 30, 1123–1135, https://doi.org/10.1175/jtech-d-12-00168.1, 2013b.

Craig, L., Moharreri, A., Rogers, D. C., Anderson, B., and Dhaniyala, S.: Aircraft-Based Aerosol Sampling in Clouds: Performance Characterization of Flow-Restriction Aerosol Inlets, J. Atmos. Ocean. Tech., 31, 2512–2521, https://doi.org/10.1175/jtech-d-14-00022.1, 2014.

Desyaterik, Y., Sun, Y., Shen, X., Lee, T., Wang, X., Wang, T., and Collett Jr., J. L.: Speciation of "brown" carbon in cloud water impacted by agricultural biomass burning in eastern China, J. Geophys. Res., 118, 7389–7399, https://doi.org/10.1002/jgrd.50561, 2013.

Di Lorenzo, R. A., Washenfelder, R. A., Attwood, A. R., Guo, H., Xu, L., Ng, N. L., Weber, R. J., Baumann, K., Edgerton, E., and Young, C. J.: Molecular-Size-Separated Brown Carbon Absorption for Biomass-Burning Aerosol at Multiple Field Sites, Environ. Sci. Technol., 51, 3128–3137, https://doi.org/10.1021/acs.est.6b06160, 2017.

Di Lorenzo, R. A., Place, B. K., VandenBoer, T. C., and Young, C. J.: Composition of Size-Resolved Aged Boreal Fire Aerosols: Brown Carbon, Biomass Burning Tracers, and Reduced Nitrogen, ACS Earth Space Chem., 2, 278–285, https://doi.org/10.1021/acsearthspacechem.7b00137, 2018.

Duarte, R. M. B. O., Pio, C. A., and Duarte, A. C.: Spectroscopic study of the water-soluble organic matter isolated from atmospheric aerosols collected under different atmospheric conditions, Anal. Chim. Acta, 530, 7–14, 2005.

Duarte, R. M. B. O., Piñeiro-Iglesias, M., López-Mahía, P., Muniategui-Lorenzo, S., Moreda-Piñeiro, J., Silva, A. M. S., and Duarte, A. C.: Comparative study of atmospheric water-soluble

organic aerosols composition in contrasting suburban environments in the Iberian Peninsula Coast, Sci. Total Environ., 648, 430–441, 2019.

Eatough, D. J., Wadsworth, A., Eatough, D. A., Crawford, J. W., Hansen, L. D., and Lewis, E. A.: A multiple system, multichannel diffusion denuder sampler for the determination of fine-particulate organic material in the atmosphere, Atmos. Environ., 27A, 1213–1219, 1993.

Echalar, F., Gaudichet, A., Cachier, H., and Artaxo, P.: Aerosol emissions by tropical forest and savanna biomass burning: Characteristic trace elements and fluxes, Geophys. Res. Lett., 22, 3039–3042, 1995.

Feng, Y., Ramanathan, V., and Kotamarthi, V. R.: Brown carbon: a significant atmospheric absorber of solar radiation?, Atmos. Chem. Phys., 13, 8607–8621, https://doi.org/10.5194/acp-13-8607-2013, 2013.

Forrister, H., Liu, J., Scheuer, E., Dibb, J., Ziemba, L., Thornhill, K. L., Anderson, B., Diskin, G., Perring, A. E., Schwarz, J. P., Campuzano-Jost, P., Day, D. A., Palm, B. B., Jimenez, J. L., Nenes, A., and Weber, R. J.: Evolution of brown carbon in wildfire plumes, Geophys. Res. Lett., 42, 4623–4630, https://doi.org/10.1002/2015GL063897, 2015.

Foster, K., Pokhrel, R., Burkhart, M., and Murphy, S.: A novel approach to calibrating a photoacoustic absorption spectrometer using polydisperse absorbing aerosol, Atmos. Meas. Tech., 12, 3351–3363, https://doi.org/10.5194/amt-12-3351-2019, 2019.

Gerbig, C., Schmitgen, S., Kley, D., Volz-Thomas, A., Dewey, K., and Haaks, D.: An improved fast-response vacuum-UV resonance fluorescence CO instrument, J. Geophys. Res., 104, 1699–1704, 1999.

Hecobian, A., Zhang, X., Zheng, M., Frank, N., Edgerton, E. S., and Weber, R. J.: Water-Soluble Organic Aerosol material and the light-absorption characteristics of aqueous extracts measured over the Southeastern United States, Atmos. Chem. Phys., 10, 5965–5977, https://doi.org/10.5194/acp-10-5965-2010, 2010.

Hems, R. F. and Abbatt, J. P. D.: Aqueous Phase Photo-oxidation of Brown Carbon Nitrophenols: Reaction Kinetics, Mechanism, and Evolution of Light Absorption, ACS Earth Space Chem., 2, 225–234, https://doi.org/10.1021/acsearthspacechem.7b00123, 2018.

Hoffer, A., Gelencsér, A., Guyon, P., Kiss, G., Schmid, O., Frank, G. P., Artaxo, P., and Andreae, M. O.: Optical properties of humic-like substances (HULIS) in biomass-burning aerosols, Atmos. Chem. Phys., 6, 3563–3570, https://doi.org/10.5194/acp-6-3563-2006, 2006.

Jacobson, M. C., Hansson, H.-C., Noone, K. J., and Charlson, R. J.: Organic atmospheric aerosols: Review and state of the science, Rev. Geophys., 38, 267–294, 2000.

Jo, D. S., Park, R. J., Lee, S., Kim, S.-W., and Zhang, X.: A global simulation of brown carbon: implications for photochemistry and direct radiative effect, Atmos. Chem. Phys., 16, 3413–3432, https://doi.org/10.5194/acp-16-3413-2016, 2016.

Kanakidou, M., Seinfeld, J. H., Pandis, S. N., Barnes, I., Dentener, F. J., Facchini, M. C., Van Dingenen, R., Ervens, B., Nenes, A., Nielsen, C. J., Swietlicki, E., Putaud, J. P., Balkanski, Y., Fuzzi, S., Horth, J., Moortgat, G. K., Winterhalter, R., Myhre, C. E. L., Tsigaridis, K., Vignati, E., Stephanou, E. G., and Wilson, J.: Organic aerosol and global climate modelling: a review, Atmos. Chem. Phys., 5, 1053–1123, https://doi.org/10.5194/acp-5-1053-2005, 2005.

Kirchstetter, T. W. and Thatcher, T. L.: Contribution of organic carbon to wood smoke particulate matter absorption of solar radiation, Atmos. Chem. Phys., 12, 6067–6072, https://doi.org/10.5194/acp-12-6067-2012, 2012.

Kirchstetter, T. W., Novakov, T., and Hobbs, P. V.: Evidence that the spectral dependence of light absorption by aerosols is affected by organic carbon, J. Geophys. Res., 109, D21208, https://doi.org/10.1029/2004JD004999, 2004.

Lack, D. A. and Langridge, J. M.: On the attribution of black and brown carbon light absorption using the Ångström exponent, Atmos. Chem. Phys., 13, 10535–10543, https://doi.org/10.5194/acp-13-10535-2013, 2013.

Lack, D. A., Langridge, J. M., Bahreini, R., Brock, C. A., Middlebrook, A. M., and Schwarz, J. P.: Brown Carbon and Internal Mixing in Biomass Burning Particles, P. Natl. Acad. Sci. USA, 109, 14802–14807, https://doi.org/10.1073/pnas.1206575109, 2012.

Langridge, J. M., Richardson, M. S., Lack, D. A., Brock, C. A., and Murphy, D. M.: Limitations of the Photoacoustic Technique for Aerosol Absorption Measurement at High Relative Humidity, Aerosol Sci. Tech., 47, 1163–1173, https://doi.org/10.1080/02786826.2013.827324, 2013.

Lee, T., Sullivan, A. P., Mack, L., Jimenez, J. L., Kreidenweis, S. M., Onasch, T. B., Worsnop, D. R., Malm, W., Wold, C. E., Hao, W. M., and Collett Jr., J. L.: Chemical smoke marker emissions during flaming and smoldering phases of laboratory open burning of wildland fuels, Aerosol Res. Lett., 44, i–v, https://doi.org/10.1080/02786826.2010.499884, 2010.

Lee, A. K. Y., Willis, M. D., Healy, R. M., Wang, J. M., Jeong, C.-H., Wenger, J. C., Evans, G. J., and Abbatt, J. P. D.: Single-particle characterization of biomass burning organic aerosol (BBOA): evidence for non-uniform mixing of high molecular weight organics and potassium, Atmos. Chem. Phys., 16, 5561–5572, https://doi.org/10.5194/acp-16-5561-2016, 2016.

Limbeck, A., Kulmala, M., and Puxbaum, H.: Secondary organic aerosol formation in the atmosphere via heterogeneous reaction of gaseous isoprene on acidic particles, Geophys. Res. Lett, 30, 1996, https://doi.org/10.1029/2003GL017738, 2003.

Liu, J., Bergin, M., Guo, H., King, L., Kotra, N., Edgerton, E., and Weber, R. J.: Size-resolved measurements of brown carbon in water and methanol extracts and estimates of their contribution to ambient fine-particle light absorption, Atmos. Chem. Phys., 13, 12389–12404, https://doi.org/10.5194/acp-13-12389-2013, 2013.

Liu, J., Scheuer, E., Dibb, J., Ziemba, L. D., Thornhill, K. L., Anderson, B. E., Wisthaler, A., Mikoviny, T., Devi, J. J., Bergin, M., and Weber, R. J.: Brown carbon in the continental troposphere, Geophys. Res. Lett., 41, 2191–2195, https://doi.org/10.1002/2013GL058976, 2014.

Liu, J., Scheuer, E., Dibb, J., Diskin, G. S., Ziemba, L. D., Thornhill, K. L., Anderson, B. E., Wisthaler, A., Mikoviny, T., Devi, J. J., Bergin, M., Perring, A. E., Markovic, M. Z., Schwarz, J. P., Campuzano-Jost, P., Day, D. A., Jimenez, J. L., and Weber, R. J.: Brown carbon aerosol in the North American continental troposphere: sources, abundance, and radiative forcing, Atmos. Chem. Phys., 15, 7841–7858, https://doi.org/10.5194/acp-15-7841-2015, 2015.

Lukács, H., Gelencsér, A., Hammer, S., Puxbaum, H., Pio, C., Legrand, M., Kasper-Giebl, A., Handler, M., Limbeck, A., Simspon, D., and Preunkert, S.: Seasonal trends and possible sources of brown carbon based on 2-year aerosol measurements at six sites in Europe, J. Geophys. Res., 112, D23S18, https://doi.org/10.1029/2006JD008151, 2007.

Marple, V. A., Rubow, K. L., and Behm, S. M.: A microorifice uniform deposit impactor (MOUDI): description, calibration, and use, Aerosol Sci. Tech., 14, 434–446, 1991.

Moharreri, A., Craig, L., Dubey, P., Rogers, D. C., and Dhaniyala, S.: Aircraft testing of the new Blunt-body Aerosol Sampler (BASE), Atmos. Meas. Tech., 7, 3085–3093, https://doi.org/10.5194/amt-7-3085-2014, 2014.

Mohr, C., Lopez-Hilfiker, F. D., Zotter, P., Prévôt, A. S. H., Xu, L., Ng, N. L., Herndon, S. C., Williams, L.R., Franklin, J. P., Zahniser, M. S., Worsnop, D. R., Knighton, W. B., Aiken, A. C., Gorkowski, K. J., Dubey, M. K., Allan, J. D., and Thornton, J. A.: Contribution of Nitrated Phenols to Wood Burning Brown Carbon Light Absoprtion in Detling, United Kingdom during Winter Time, Environ. Sci. Technol., 47, 6316–6324, 2013.

Moosmüller, H., Chakrabarty, R. K., and Arnott, W. P.: Aerosol light absorption and its measurement: A review, J. Quant. Spectrosc. Ra., 110, 844–878, https://doi.org/10.1016/j.jqsrt.2009.02.035, 2009.

Murphy, S.: Aerosol Extinction, Scattering and Absorption (PAS CAPS) Data, Version 1.0, UCAR/NCAR – Earth Observing Laboratory [data set], https://doi.org/10.26023/K8P0-X4T3-TN06, 2019 (data available at: http://data.eol.ucar.edu/master_lists/generated/we-can/, last access: 14 June 2019).

Orsini, D. A., Ma, Y., Sullivan, A., Sierau, B., Baumann, K., and Weber, R. J.: Refinements to the particle-into-liquid sampler (PILS) for ground and airborne measurements of water-soluble aerosol composition, Atmos. Environ., 37, 1243–1259, 2003.

Palm, B. B., Peng, Q., Fredrickson, C. D., Lee, B. H., Garofalo, L. A., Pothier, M. A., Kreidenweis, S. M., Farmer, D. K., Pokhrel, R. P., Shen, Y., Murphy, S. M., Permar, W., Hu, L., Campos, T. L., Hall, S. R., Ullmann, K., Zhang, X., Flocke, F., Fischer, E. V., and Thornton, J. A.: Quantification of organic aerosol and brown carbon evolution in fresh wildfire plumes, P. Natl. Acad. Sci. USA, 117, 29469–29477, https://doi.org/10.1073/pnas.2012218117, 2020.

Pokhrel, R. P., Beamesderfer, E. R., Wagner, N. L., Langridge, J. M., Lack, D. A., Jayarathne, T., Stone, E. A., Stockwell, C. E., Yokelson, R. J., and Murphy, S. M.: Relative importance of black carbon, brown carbon, and absorption enhancement from clear coatings in biomass burning emissions, Atmos. Chem. Phys., 17, 5063–5078, https://doi.org/10.5194/acp-17-5063-2017, 2017.

Saleh, R., Hennigan, C. J., McMeeking, G. R., Chuang, W. K., Robinson, E. S., Coe, H., Donahue, N. M., and Robinson, A. L.: Absorptivity of brown carbon in fresh and photo-chemically aged biomass-burning emissions, Atmos. Chem. Phys., 13, 7683–7693, https://doi.org/10.5194/acp-13-7683-2013, 2013.

Sareen, N., Schwier, A. N., Shapiro, E. L., Mitroo, D., and McNeill, V. F.: Secondary organic material formed by methylglyoxal in aqueous aerosol mimics, Atmos. Chem. Phys., 10, 997–1016, https://doi.org/10.5194/acp-10-997-2010, 2010.

Saxena, P. and Hildemann, L. M.: Water-soluble organics in atmospheric particles: A critical review of the literature and applications of thermodynamics to identify candidate compounds, J. Atmos. Chem., 24, 57–109, 1996.

Schauer, J. J., Kleeman, M. J., Cass, G. R., and Simoneit, B. R. T.: Measurement of Emissions from Air Pollution Sources. 3. C_1–C_{29} Organic Compounds from Fireplace Combustion of Wood, Environ. Sci. Technol., 35, 1716–1728, 2001.

Simoneit, B. R. T., Schauer, J. J., Nolte, C. G., Oros, D. R., Elias, V. O., Fraser, M. P., Rogge, W. F., and Cass, G. R.: Levoglucosan, a tracer for cellulose in biomass burning and atmospheric particles, Atmos. Environ., 33, 173–182, 1999.

Sorooshian, A., Brechtel, F. J., Ma, Y., Weber, R. J., Corless, A., Flagan, R. C., and Seinfeld, J. H.: Modeling and Characterization of a Particle-into-Liquid Sampler (PILS), Aerosol Sci. Tech., 40, 396–409, 2006.

Sullivan, A.: Particle Into Liquid Sampler 1 (PILS1) Three second integrated WSOC Data, Version 1.0, UCAR/NCAR – Earth Observing Laboratory [data set], https://doi.org/10.26023/9H07-MD9K-430D, 2019 (data available at: http://data.eol.ucar.edu/master_lists/generated/we-can/, last access: 4 March 2019).

Sullivan, A.: Particle Into Liquid Sampler 1 (PILS1) Sixteen second integrated Abs365, Version 2.0, UCAR/NCAR – Earth Observing Laboratory [data set], https://doi.org/10.26023/CRHY-NDT9-C30V, 2021a (data available at: http://data.eol.ucar.edu/master_lists/generated/we-can/, last access: 21 March 2021).

Sullivan, A.: Particle Into Liquid Sampler 2 (PILS2) two minute integrated cations, anions, levoglucosan, and organic acids data, Version 1.0, UCAR/NCAR – Earth Observing Laboratory [data set], https://doi.org/10.26023/7TAN-TZMD-680Y, 2021b (data available at: http://data.eol.ucar.edu/master_lists/generated/we-can/, last access: 21 March 2021).

Sullivan, A. P., Peltier, R. E., Brock, C. A., de Gouw, J. A., Holloway, J. S., Warneke, C., Wollny, A. G., and Weber, R. J.: Airborne measurements of carbonaceous aerosol soluble in water over northeastern United States: Method development and an investigation into water-soluble organic carbon sources, J. Geophys. Res., 111, D23S46, https://doi.org/10.1029/2006JD007072, 2006.

Sullivan, A. P., Frank, N., Kenski, D. M., and Collett Jr, J. L.: Application of High-Performance Anion-Exchange Chromatography – Pulsed Amperometric Detection for Measuring Carbohydrates in Routine Daily Filter Samples Collected by a National Network: 2. Examination of Sugar Alcohols/Polyols, Sugars, and Anhydrosugars in the Upper Midwest, J. Geophys. Res., 116, D08303, https://doi.org/10.1029/2010JD014169, 2011a.

Sullivan, A. P., Frank, N., Onstad, G., Simpson, C. D., and Collett Jr., J. L.: Application of High-Performance Anion-Exchange Chromatography – Pulsed Amperometric Detection for Measuring Carbohydrates in Routine Daily Filter Samples Collected by a National Network: 1. Determination of the Impact of Biomass Burning in the Upper Midwest, J. Geophys. Res., 116, D08302, https://doi.org/10.1029/2010JD014166, 2011b.

Sullivan, A. P., May, A. A., Lee, T., McMeeking, G. R., Kreidenweis, S. M., Akagi, S. K., Yokelson, R. J., Urbanski, S. P., and Collett Jr., J. L.: Airborne characterization of smoke marker ratios from prescribed burning, Atmos. Chem. Phys., 14, 10535–10545, https://doi.org/10.5194/acp-14-10535-2014, 2014.

Sullivan, A. P., Guo, H., Schroder, J. C., Campuzano-Jost, P., Jimenez, J. L., Campos, T., Shah, V., Jaeglé, L., Lee, B. H., Lopez-Hilfiker, F. D., Thornton, J. A., Brown, S. S., and We-

ber, R. J.: Biomass Burning Markers and Residential Burning in the WINTER Aircraft Campaign, J. Geophys. Res.-Atmos., 124, 1846–1861, https://doi.org/10.1029/2017JD028153, 2019.

Sumlin, B. J., Pandey, A., Walker, M. J., Pattison, R. S., Williams, B. J., and Chakrabarty, R. K.: Atmospheric Photooxidation Diminishes Light Absorption by Primary Brown Carbon Aerosol from Biomass Burning, Environ. Sci. Tech. Lett., 4, 540–545, https://doi.org/10.1021/acs.estlett.7b00393, 2017.

Toohey, D.: CVI/UHSAS Data, Version 1.1, UCAR/NCAR – Earth Observing Laboratory [data set], https://doi.org/10.26023/BZ4F-EAC4-290W, 2019 (data available at: http://data.eol.ucar.edu/master_lists/generated/we-can/, last access: 14 June 2019).

UCAR/NCAR – Earth Observing Laboratory: WE-CAN: Low Rate (LRT – 1 sps) Navigation, State Parameter, and Microphysics Flight-Level Data – ICARTT format, Version 1.1, UCAR/NCAR – Earth Observing Laboratory [data set], https://doi.org/10.26023/G766-BS71-9V03, 2019 (data available at: http://data.eol.ucar.edu/master_lists/generated/we-can/, last access: 6 May 2019).

Updyke, K. M., Nguyen, T. B., and Nizkorodov, S. A.: Formation of brown carbon via reactions of ammonia with secondary organic aerosols from biogenic and anthropogenic precursors, Atmos. Environ., 63, 22–31, 2012.

Verma, V., Wang, Y., El-Afifi, R., Fang, T., Rowland, J., Russell, A. G., and Weber, R. J.: Fractionating ambient humic-like substances (HULIS) for their reactive oxygen species activity – Assessing the importance of quinones and atmospheric aging, Atmos. Environ., 120, 351–359, 2015.

Washenfelder, R. A., Azzarello, L., Ball, K., Brown, S. S., Decker, Z. C. J., Franchin, A., Fredrickson, C. D., Hayden, K., Holmes, C. D., Middlebrook, A. M., Palm, B. B., Pierce, R. B., Price, D. J., Roberts, J. M., Robinson, M. A., Thornton, J. A., Womack, C. C., and Young, C. J.: Complexity in the Evolution, Composition, and Spectroscopy of Brown Carbon in Aircraft Measurements of Wildfire Plumes, Geophys. Res. Lett., 49, e2022GL098951, https://doi.org/10.1029/2022GL098951, 2022.

Ward, D. E. and Radke, L. F.: Emission measurements from vegetation fires: a comparative evaluation of methods and results, in: Fire in the environment: the ecological, atmospheric, and climatic importance of vegetation fires, edited by: Crutzen, P. J. and Goldammer, J. G., Wiley, Chichester, England, 53–76, 1993.

Ward, D. E., Setzer, A. W. Kaufman, Y. J., and Rasmussen, R. A.: Characteristics of smoke emissions from biomass fires of the Amazon region-BASE-A experiment, in: Global Biomass Burning: Atmospheric, Climatic, and Biospheric Implications, edited by: Levine, J. S., MIT Press, Cambridge, MA, 394-402, 1991.

Wong, J. P. S., Tsagkaraki, M., Tsiodra, I., Mihalopoulos, N., Violaki, K., Kanakidou, M., Sciare, J., Nenes, A., and Weber, R. J.: Atmospheric evolution of molecular-weight-separated brown carbon from biomass burning, Atmos. Chem. Phys., 19, 7319–7334, https://doi.org/10.5194/acp-19-7319-2019, 2019.

Yttri, K. E., Aas, W., Bjerke, A., Cape, J. N., Cavalli, F., Ceburnis, D., Dye, C., Emblico, L., Facchini, M. C., Forster, C., Hanssen, J. E., Hansson, H. C., Jennings, S. G., Maenhaut, W., Putaud, J. P., and Tørseth, K.: Elemental and organic carbon in PM10: a one year measurement campaign within the European Monitoring and Evaluation Programme EMEP, Atmos. Chem. Phys., 7, 5711–5725, https://doi.org/10.5194/acp-7-5711-2007, 2007.

Zeng, L., Zhang, A., Wang, Y., Wagner, N. L., Katich, J. M., Schwarz, J. P., Schill, G. P., Brock, C., Froyd, K. D., Murphy, D. M., Williamson, C. J., Kupac, A., Scheuer, E., Dibb, J., and Weber, R. J.: Global Measurements of Brown Carbon and Estimated Direct Radiative Effects, Geophys. Res. Lett., 47, e2020GL088747, https://doi.org/10.1029/2020GL088747, 2020.

Zeng, L., Dibb, J., Scheuer, E., Katich, J. M., Schwarz, J. P., Bourgeois, I., Peischl, J., Ryerson, T., Warneke, C., Perring, A. E., Diskin, G. S., DiGangi, J. P., Nowak, J. B., Moore, R. H., Wiggins, E. B., Pagonis, D., Guo, H., Campuzano-Jost, P., Jimenez, J. L., Xu, L., and Weber, R. J.: Characteristics and evolution of brown carbon in western United States wildfires, Atmos. Chem. Phys., 22, 8009–8036, https://doi.org/10.5194/acp-22-8009-2022, 2022.

Zhang, A., Wang, Y., Zhang, Y., Weber, R. J., Song, Y., Ke, Z., and Zou, Y.: Modeling the global radiative effect of brown carbon: a potentially larger heating source in the tropical free troposphere than black carbon, Atmos. Chem. Phys., 20, 1901–1920, https://doi.org/10.5194/acp-20-1901-2020, 2020.

Zhang, Q., Jimenez, J. L., Canagaratna, M. R., Allan, J. D., Coe, H., Ulbrich, I., Alfarra, M. R., Takami, A., Middlebrook, A. M., Sun, Y. L., Dzepina, K., Dunlea, E., Docherty, K., DeCarlo, P. F., Salcedo, D., Onasch, T., Jayne, J. T., Miyoshi, T., Shimono, A., Hatakeyama, S., Takegawa, N., Kondo, Y., Schneider, J., Drewnick, F., Borrmann, S., Weimer, S., Demerjian, K., Williams, P., Bower, K., Bahreini, R., Cottrell, L., Griffin, R. J., Rautiainen, J., Sun, J. Y., Zhang, Y. M., and Worsnop, D. R.: Ubiquity and dominance of oxygenated species in organic aerosols in anthropogenically-influenced Northern Hemisphere midlatitudes, Geophys. Res. Lett., 34, L13801, https://doi.org/10.1029/GL029979, 2007.

Zhang, X., Lin, Y.-H., Surratt, J. D., Zotter, P., Prévôt, A. S. H., and Weber, R. J.: Light-absorbing soluble organic aerosol in Los Angeles and Atlanta: A contrast in secondary organic aerosol, Geophys. Res. Lett., 38, L21810, https://doi.org/10.1029/2011GL049385, 2011.

Zhang, X., Lin, Y.-H., Surratt, J. D., and Weber, R. J.: Sources, Composition and Absorption Ångström Exponent of Light-absorbing Organic Components in Aerosol Extracts from the Los Angeles Basin, Environ. Sci. Technol., 47, 3685–3693, https://doi.org/10.1021/es305047b, 2013.

Zhang, Y., Forrister, H., Liu, J., Dibb, J., Anderson, B., Schwarz, J. P., Perring, A. E., Jimenez, J. L., Campuzano-Jost, P., Wang, Y., Nenes, A., and Weber, R. J.: Top-of-atmosphere radiative forcing affected by brown carbon in the upper troposphere, Nat. Geosci., 10, 486–489, https://doi.org/10.1038/NGEO2960, 2017.

Zhao, R., Lee, A. K. Y., Huang, L., Li, X., Yang, F., and Abbatt, J. P. D.: Photochemical processing of aqueous atmospheric brown carbon, Atmos. Chem. Phys., 15, 6087–6100, https://doi.org/10.5194/acp-15-6087-2015, 2015.

Zhong, M. and Jang, M.: Dynamic light absorption of biomass-burning organic carbon photochemically aged under natural sunlight, Atmos. Chem. Phys., 14, 1517–1525, https://doi.org/10.5194/acp-14-1517-2014, 2014.